Bioimpedance real-time charazterization of neointimal tissue inside stents

D. Rivas-Marchena, A. Olmo, G. Huertas, A. Yúfera
Faculty of Physics and Computer Eng. School (ETSII)
University of Seville, Av. Reina Mercedes s/n
41012 Seville, Spain
david.rivas-marchena@ieee.org, {aolmo1,gloria,yufera}@us.es

J. A. Miguel, M. Martinez
Microelectronics Engineering Group
University of Cantabria, Av. de los Castros s/n
39005 Santander, Spain
{jamd,martinez}@teisa.unican.es

Abstract—It is hereby presented a new approach to monitor restenosis in arteries fitted with a stent during an angioplasty. The growth of neointimal tissue is followed up by measuring its bioimpedance with Electrical Impedance Spectroscopy (EIS). Besides, a mathematical model is derived to analytically describe the neointima's histological composition from its bioimpedance. The model is validated by finite-element analysis (FEA) with COMSOL Multiphysics®. Satisfactory correlation between the analytical model and the FEA simulation is achieved for most of the characterization range, detecting some deviations introduced by the thin "double layer" that separates the neointima and the blood. It is shown how to apply conformal transformations to obtain bioimpedance models for stack-layered tissues over coplanar electrodes. Particularly, this is applied to characterize the neointima in real-time. This technique is either suitable as a main mechanism of restenosis follow-up or it can be combined with proposed blood-pressure-measuring intelligent stents to auto-calibrate the sensibility loss caused by the adherence of the tissue on the micro-electro-mechanical sensors (MEMS).

Keywords—*Arteriosclerosis, BioImpedance, Cardiology, Medical test, Neointima, Oscillation-Based Test (OBT).*

I. INTRODUCTION

Ischemic heart disease is the leading cause of morbidity and mortality in the World [1,2]. The interior of the elastic and muscular arteries shrinks (stenosis), mainly by the growth of a lipid layer (atherosclerosis), causing angina chest pain and acute myocardial infarction. Among the existing treatments, the most popular employs a flexible metal mesh (stent) to mechanically support the opening of stenotic segments and ensure permeability [3-4]. However, despite improvements on the surgery techniques and the stent design [5], there is a high probability of medium-term restenosis [6].

It was proposed to use micro-electro-mechanical (MEMs) pressure sensors to monitor restenosis with intelligent-stents [7]. The sensors are implemented as parallel-plate capacitors: one plate fixed, the other bends with increasing pressure. The distance between plates determines a capacitance that is read out with an electronic circuit [8]. However, the growth of the neointimal tissue on top of the flexible plate compromises its flexibility and degrades the sensor sensitivity.
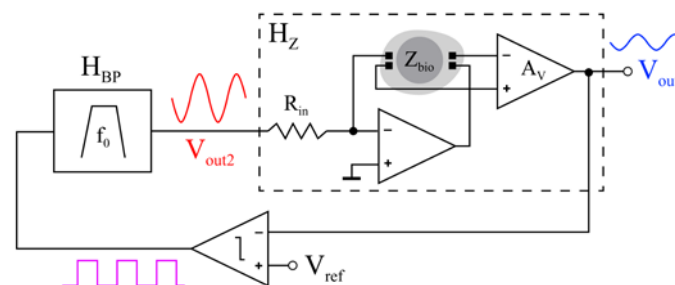
Fig. 1. Bioimpedance self-stimulated monitoring system based on OBT [5].

Characterizing the neointima would ease the integration of a calibration block to compensate the sensitivity loss [9]. Recent publications already use bioimpedance techniques to follow up the restenosis by studying the growth of new tissue on the artery (neointimal layer). Some solutions provide the catheter with a matrix of microelectrodes [10], [11]. Others place the electrodes straightaway on the stent [12]. It has been also shown how to use the stent itself as a big electrode [13]. These alternatives do not reduce patient risk though. They still rely on catheterization to link external measuring equipment.

There is a published method to monitor cell-cultures *in vivo* based on their bioimpedance [14]. It consists on converting the Cell-Culture Under Test (CCUT) into a "biological oscillator" whose parameters (e.g., frequency, amplitude, and phase) are related to the cell-culture evolution. This approach, known as Oscillation-Based Test (OBT), is also valid to monitor the growth of neointima. A system topology as shown in Fig. 1 amplifies the bioimpedance and limits the amplitude of the output signal with a non-linear comparator. To close the loop, a filter sets a quasi-sinusoidal signal to stimulate the tissue. The input resistor keeps the current injected to the blood vessel within safety margins. At the node *Vout2* the oscillation is analyzed and all the relevant parameters are extracted.

A robust and thorough neointimal model is essential to link the experimental results with the variations in the tissue layers comprising it. This paper is primarily focused on the development of such an analytical model (Section II), its validation against Finite-Element Analysis (FEA) simulations (Section III), and an early proof-of-concept of its applicability in conjunction with OBT (Section IV). Finally, some conclusions follow on Section V.

II. ANALYTICAL MODEL

The neointima bioimpedance depends on the thickness of the tissue layers that comprise it – lipid core, smooth muscle, fiber cap and endothelium. They are assumed to be stacked in parallel and immersed in blood as in Fig. 2.a. The effect of the electrodes on the final impedance is dismissed because of the chosen four-electrodes topology [15]. They are placed around the MEMS pressure sensor as shown in Fig. 2.b to maximize the transference impedance [16].

A. Neointima-Blood interface ("double layer")

The blood is an electrolyte – it has free charge carriers – but the cellular structure immobilizes charge in the neointima. The difference between the media produces a charge zone where the blood ions that are closer to the interface are fixed by the outermost tissue layer [16]. This charge zone extends through the electrolyte, creating what is known as "double layer" – a capacitor to be included in the analytical model. This effect is described with a triple-layer model [17] that results in a ε_r=17.8 and a Debye length of 0.64 nm – four to five orders of magnitude smaller than usual tissue thicknesses.
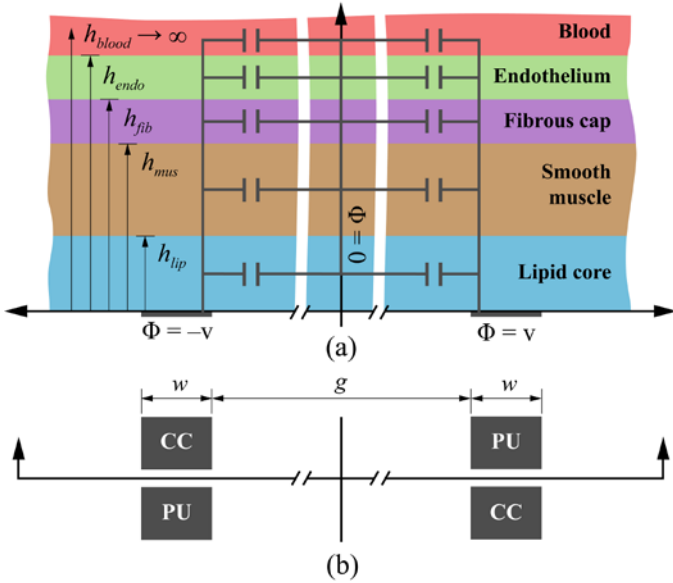

Fig. 2. (a) Stack of neointimal tissue layers and parallel partial capacitances. (b) Layout of current-carrying (CC) and pick-up (PU) electrodes.
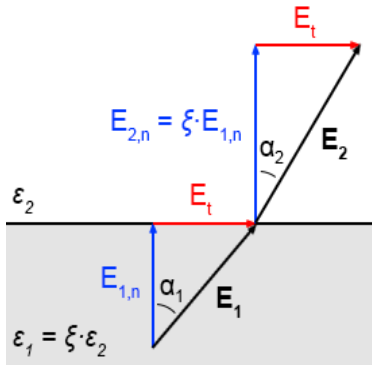

Fig. 3. Electric field angle change in a dielectric interface.

B. Dielectric interface

From the set of Maxwell equations, it is derived that the electric field angle in a dielectric interface (Fig. 3) changes as

$$\frac{\tan \alpha_2}{\tan \alpha_1} = \frac{\mathbf{E_{2,t}}/\mathbf{E_{2,n}}}{\mathbf{E_{1,t}}/\mathbf{E_{1,n}}} = \frac{\mathbf{E_{1,n}}}{\mathbf{E_{2,n}}} = \frac{\mathbf{D_{1,n}}/\varepsilon_1}{\mathbf{D_{2,n}}/\varepsilon_2} = \frac{\varepsilon_2}{\varepsilon_1} . \quad (1)$$

where $\mathbf{E_{i,t}}$ and $\mathbf{E_{i,n}}$ are the tangential and normal components of the electric field and $\mathbf{D_{i,n}}$ are the normal components of the electric displacement for each dielectric.

For interfaces where the media permittivity varies largely, two different boundary conditions may apply:

- Dirichlet Boundary Condition (DBC), for $\varepsilon_2 \gg \varepsilon_1$, with constant electric potential at the interface (Φ=0).

- Neumann Boundary Condition (NBC), for $\varepsilon_2 \ll \varepsilon_1$, with no potential gradient normal to the interface ($\partial\Phi/\partial\mathbf{n}$=0).

C. Partial Capacitance (PC) method

Ghione and Goano [18] showed that the total capacitance between coplanar tracks in PCBs can be derived from the contribution of each layer of material in parallel with them.

The electrodes of the intelligent-stent are so close compared to the stent diameter that they can also be assumed coplanar and the neointima stratified in parallel layers on top (Fig. 2.a).

If permittivity decreases with the distance to the electrodes, all the dielectric interfaces can be modelled with Neumann boundary conditions (NBC). Then, the partial capacitances are effectively connected in parallel (PPC), so the equivalent is

$$C_{eq} = \sum_{i=1}^{i=n-1} \left[\varepsilon_{r,i} - \varepsilon_{r,i+1} \right] C_{PPC}(h_i) + \varepsilon_{r,n} C(\infty) \quad (2)$$

where n is the number of layers, h_i is the height of each layer measured from the electrodes plane and $C_{PPC}(h_i)$ is the void capacitance of each layer limited by a NBC.

Conversely, if permittivity increases, the capacitances are assumed in series (SPC) with DBCs in the interfaces. Then,

$$\frac{1}{C_{eq}} = \sum_{i=1}^{i=n-1} \left[\frac{1}{\varepsilon_{r,i}} - \frac{1}{\varepsilon_{r,i+1}} \right] \frac{1}{C_{SPC}(h_i)} + \frac{1}{\varepsilon_{r,n}} \frac{1}{C(\infty)} . \quad (3)$$

Since the plates of these capacitors – the electrodes – are coplanar, there is no simple formula to compute capacitances. To cope with this, Igreja and Dias [19] applied conformal mapping techniques to transform the disposition of electrodes into a parallel-plate configuration whose capacitance is:

$$C_{partial} = \varepsilon_r \, \varepsilon_0 \, L \frac{K(k)}{K(k')} \quad (4)$$

depending on the tissue relative permittivity ε_r, the electrodes depth L and the equivalent width after spatial transformations, as a ratio of complete elliptic integrals of the first kind (K) with modulus k (Table 1) and its complementary $k'=\sqrt{(1-k^2)}$.

TABLE I.   CONFORMAL MAPPING PARAMETERS [15]

Series Partial Capacitance (SPC)	Parallel Partial Capacitance (PPC)
$k_{SPC} = \sqrt{\dfrac{t_4 - t_3}{t_4 - 1}}$	$k_{PPC} = \dfrac{1}{t_3}\sqrt{\dfrac{t_4^2 - t_3^2}{t_4^2 - 1}}$
$t_3 = \cosh\left(\dfrac{\pi(1-\eta)}{4r}\right)$	$t_3 = \cosh\left(\dfrac{\pi(1-\eta)}{8r}\right)$
$t_4 = \cosh\left(\dfrac{\pi(1+\eta)}{4r}\right)$	$t_4 = \cosh\left(\dfrac{\pi(1+\eta)}{8r}\right)$
$\eta = w/(w+g)$	
$r = 2h/(w+g)$	

In the equations, w and g are the width of the electrodes and the gap between them, respectively, and h is the height of a given tissue layer.

D. Iterative complex method

The proposed partial capacitance method is only valid for stacks of material whose permittivities vary monotonically. Blume [20] published an iterative method compatible with any kind of stack, in terms of permittivity, that groups layers in pairs and computes equivalent permittivities sequentially:

$$\text{SPC:}\quad \varepsilon_{eq,i} = \frac{\varepsilon_{eq,i-1}\,\varepsilon_{i+1}\,\kappa(h_i)}{\kappa(h_{i+1})\left(\varepsilon_{i+1} - \varepsilon_{eq,i-1}\right) + \varepsilon_{eq,i-1}\,\kappa(h_i)} \quad (5)$$

$$\text{PPC:}\quad \varepsilon_{eq,i} = \left(\varepsilon_{eq,i-1} - \varepsilon_{i+1}\right)\frac{\kappa(h_i)}{\kappa(h_{i+1})} + \varepsilon_{i+1} \quad (6)$$

where $\kappa = K(k)/K(k')$ is used to simplify the expressions.

By replacing the permittivity with the complex permittivity ($\varepsilon^* = \varepsilon - j\sigma/\omega$), the iterative method can include resistances into the model, and therefore calculate the equivalent impedance of any stack of parallel layers of tissue as

$$Z = j\omega \Big/ \left[L\,\kappa(\infty)\,\varepsilon_{eq,n-1}^*\right]. \quad (7)$$

A diagram of the iterative method is shown in Fig. 4. This is implemented in MATLAB® using mainly the permittivity and conductivity data provided by Gabriel and Gabriel [21].
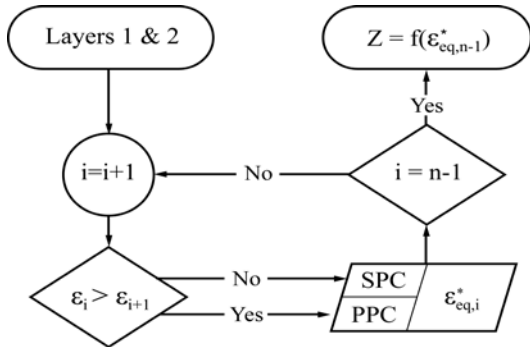

Fig. 4.   Iterative method to derive the analytical bioimpedance model.

TABLE II.   HISTOLOGICAL CONFIGURATIONS

Config.	Neointimal tissue layer thickness (µm)			
	Lipid core	Muscle	Fibrous cap	Endothelium
1	0	25	0	10
2	0	50	0	10
3	25	50	5	10
4	50	100	10	10
5	100	100	20	10
6	200	100	40	10

The comparison of permittivities (Fig. 5) determines in which frequency ranges is applicable SPC or PPC. Therefore, the accuracy is expected bigger for $\varepsilon_2 \gg \varepsilon_1$ or $\varepsilon_2 \ll \varepsilon_1$ (clear boundary conditions) and for $\varepsilon_2 \approx \varepsilon_1$ (nearly no interface) [11].

The increment in total thickness after adding the "double layer" is quite small. This leads to similar elliptic integrals whose difference is comparable to the calculation error. Hence, the model needs experimental adjustment to be accurate.

III.   FINITE-ELEMENT ANALYSIS (FEA) SIMULATION

The analytical bioimpedance model described in Section II is verified against Finite-Element Analysis (FEA) with COMSOL Multiphysics®. Several sample configurations try to represent the growth of neointimal tissue (Table II).

To include the "double layer" in the simulation, it has been considered that the permittivity of the endothelium is much larger than the one derived for the "double layer" (ε_r=17.8). This charge-zone effect can be modelled as an impedance contact condition between the endothelium and the blood [22].
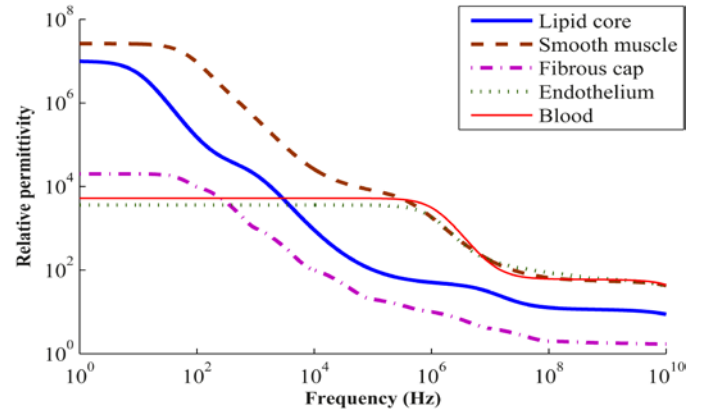

Fig. 5.   Relative permittivity data versus frequency for the blood and the tissues considered in the model.
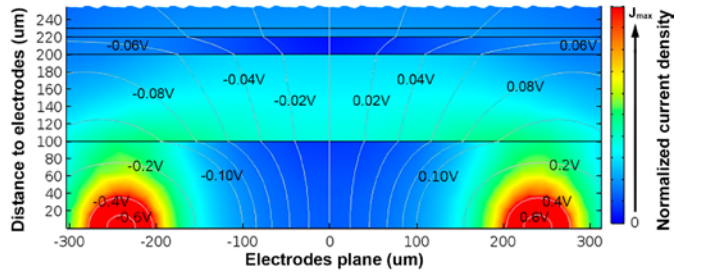

Fig. 6.   Results of 2D FEA simulation for config. 5 in Table II. Color plane represents normalized current density. Grey lines are equipotential (V).

The simplest model of the system is a 2D cross-section. This replicates the geometry employed for the mathematical transformations. The same assumptions made during the theoretical analysis are repeated here (i.e., no border effects, same electric fields and current in all the cross-sections, etc.). Thus, the validity of the bioimpedance can be easily proved against a simulation with the same limitations.

Only two electrodes are modelled, with no thickness, to dismiss the perturbation their interface with the neointima would introduce. Note that this perturbation is theoretically avoided with the four-electrodes configuration chosen. These electrodes are used both for injecting AC voltage to stimulate the tissues and to pick up the bioimpedance – derived by integrating along the current lines between electrodes.

IV. RESULTS

A. Analytical and FEA simulation comparison

The iterative analytical method is applied successfully for the six configurations of neointimal histology in Table II. In Fig. 7.a it is compared the analytical and simulated permittivity and conductivity of the neointima. The relative error is small and within the expected accuracy, given the errors in mathematical transformations and ideal boundary conditions.

The final equivalent bioimpedance is derived by computing also the effect of the blood. At this stage, an experimental adjustment is required to overcome the limitations of handling thin layers like the "double layer", as mentioned in Section III.
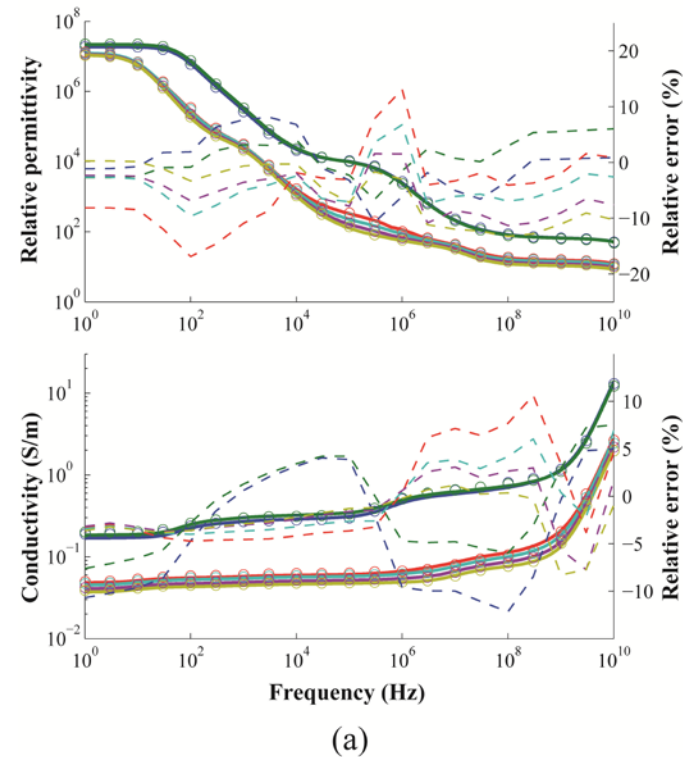
In Fig. 7.b it is shown the analytical model and the 2D FEA simulation results. There is a negligible deviation in magnitude but larger relative difference in phase.

B. Generalization of the bioimpedance model

So far, the analytical model requires to execute the iterative method for each histological configuration. However, based on several samples, it can be derived a general expression for the bioimpedance model in terms of its frequency dependence. Due to the shape of the frequency responses, it is assumed to have a gain, three poles and three zeroes, like:

$$Z_{eq}(s = j\omega) = A \frac{(s + z_1)(s + z_2)(s + z_3)}{(s + p_1)(s + p_2)(s + p_3)} \quad (8)$$

By running least-squares fitting on the data samples a zero is fixed at 20 GHz whereas the gain, poles remaining zeroes depend linearly on the thickness of each neointimal tissue:

$$x = \alpha_1 d_{lip} + \alpha_2 d_{mus} + \alpha_3 d_{fib} + \alpha_4 \quad (9)$$

where x is the parameter (gain, pole or zero), α_i are the linear coefficients and $\underline{d}_i$ are the thickness of lipid, muscle and fiber.

Different linear coefficients are derived for histological configurations without neo-atherosclerosis (i.e., no lipid core nor fibrous cap) on Table III and with it on Table IV.
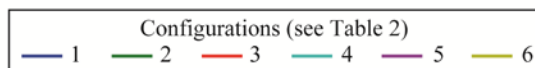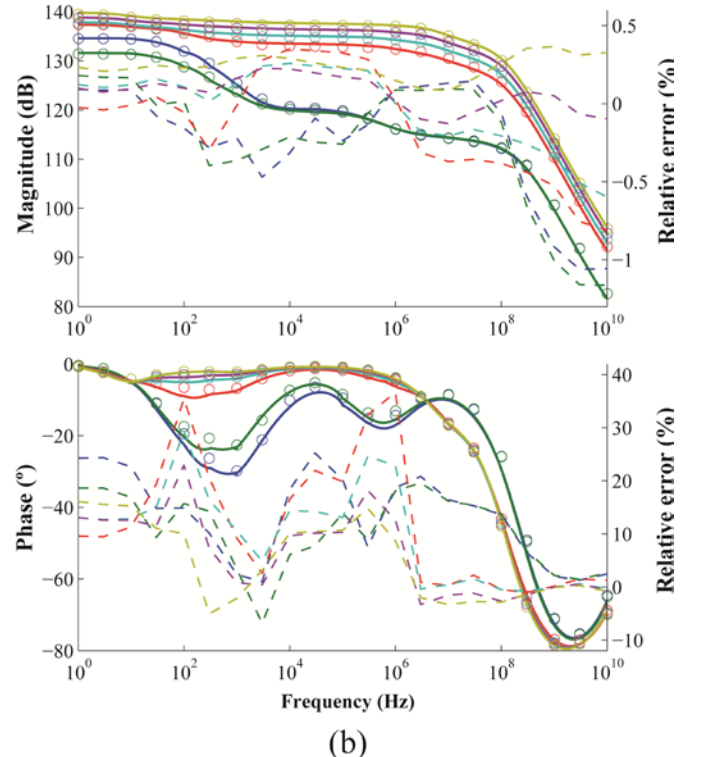

Fig. 7. Analytical model (circles) and 2D FEA simulation (solid); relative error in dashed lines – (a) relative permittivity and conductivity; (b) bioimpedance.

| Param. | Coefficient for (9) related to tissue layers | | | |
	Lipid core (α1)	Muscle (α2)	Fibrous cap (α3)	Independent (α4)
A	—	4.60e–1	—	1.72e+2
p1	—	–1.17e+1	—	4.52e+2
p2	—	2.45e+3	—	1.82e+6
p3	—	2.56e+6	—	8.59e+8
z1	—	2.30e–1	—	6.28e+2
z2	—	–9.72e+3	—	4.24e+6

| Param. | Coefficient for (9) related to tissue layers | | | |
	Lipid core (α1)	Muscle (α2)	Fibrous cap (α3)	Independent (α4)
A	1.17e+0	4.41e+0	2.30e–1	4.14e+2
p1	–1.70e–1	–9.50e–1	–3.00e–2	2.24e+2
p2	3.02e+4	1.80e+5	6.03e+3	1.36e+7
p3	4.40e+4	2.99e+5	8.80e+3	5.46e+8
z1	–2.10e–1	–1.23e+0	–4.00e–2	2.80e+2
z2	–4.79e+4	2.86e+5	9.57e+3	1.97e+7

| Config. | Neointimal tissue layer thickness (µm) | | | |
	Lipid core	Muscle	Fibrous cap	Endothelium
1	0	25	0	10
2	0	50	0	10
3	0	100	0	10
4	0	200	0	10
5	25	50	5	10
6	100	50	20	10
7	300	50	50	10
8	50	100	10	10
9	100	100	20	10
10	200	100	40	10

C. Oscillation-Based Test (OBT) auto-calibration circuit

The set of histological configurations is enlarged (Table V). It recreates the usual case where the patient firstly develops a neointima without atherosclerosis. Then, two subsets of configurations with neo-atherosclerosis show the growth of fibrous cap over thin and thick muscle layers.

An interesting frequency range to implement the OBT is around 70 Hz, since there are large phase variations in this area as depicted in Fig. 8. The OBT loop depicted in Fig. 1 is implemented in MATLAB® for this frequency as in [14]. The changes in neointimal histology cause the variations in oscillation amplitude and frequency shown in Fig. 9.

These results prove easy to determine cases where the patient has developed neo-atherosclerosis just by measuring if the oscillation frequency is above or under the nominal value. Besides, changes in amplitude help to distinguish the growth of different neointimal tissue layers. The frequency range can be enlarged by changing the quality factor of the band-pass filter. Despite the absolute accuracy of the bioimpedance model may not be enough for some applications, it tracks properly incremental changes of the neointima. Hence, this model is completely applicable to the auto-calibration of stents [12].
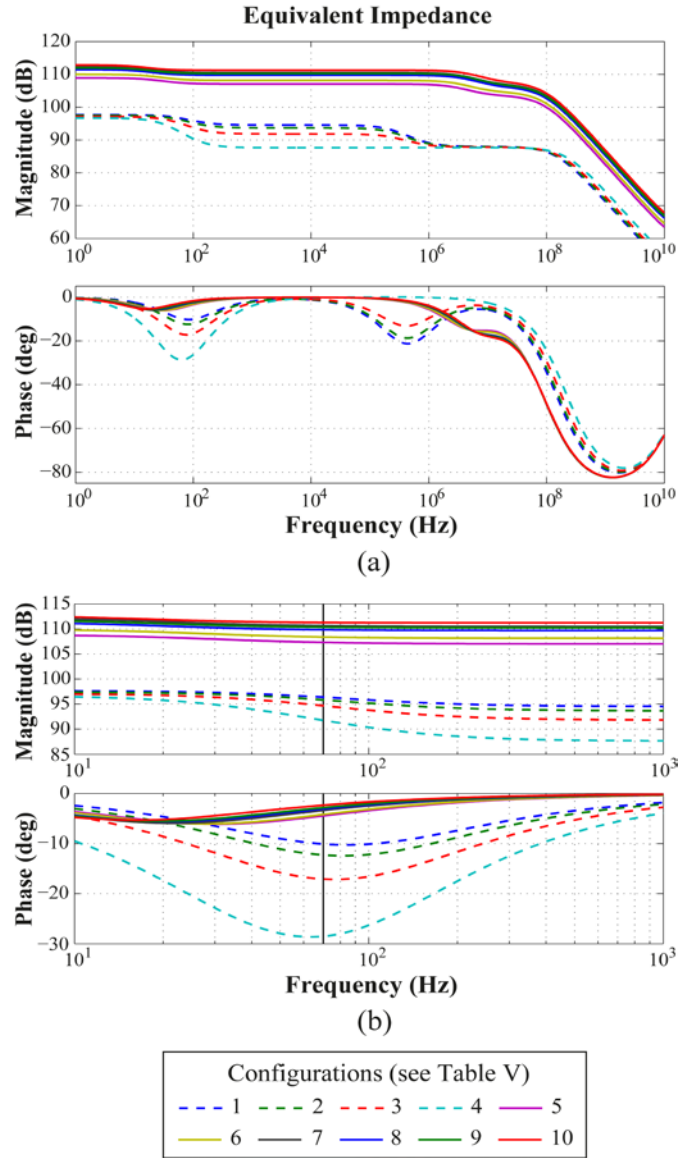

Fig. 8.   Neointima bioimpedance – (a) Bode plot; (b) detail around 70 Hz.
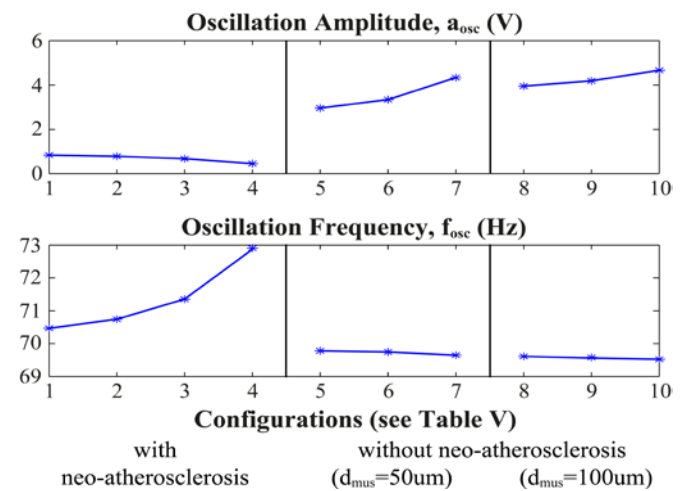

Fig. 9.   Amplitude and frequency of OBT auto-calibration circuit for the histological configurations of Table V, measured at Vout2 in Fig. 1.

V. Conclusion

It has been presented an analytical method to obtain the bioimpedance of a parallel-stack of tissues over coplanar electrodes, depending on the thickness of each layer and their electromagnetic properties. We employed an iterative approach based on conformal spatial transformations. The correlation obtained between the analytic model of the bioimpedance and 2D FEA simulation results is enough to consider the model a reasonable predictor of variations in the histology of the neointima. It permits distinguishing patients with or without neo-atherosclerosis and track the evolution of the tissue with reasonable accuracy and minimum computational cost.

The oscillation-based technique proposed provides a direct procedure to generate amplitude and frequency signals, dependent on neointimal tissue composition. This capability is applied to monitoring the restenosis with intelligent-stents, providing input data to a real-time auto-calibration of the MEMS sensors used.

Further work is required to improve the overall system accuracy, and predict precise absolute values. It is also desired to include the effects, such as border effects, anisotropy and other 3D non-idealities. Finally, it is needed a workaround to incorporate the very thin layers as the "double layer" to the analytical model.

References

[1] OECD/EU, Health at a Glance: Europe 2016: State of Health in the EU Cycle, *OECD Publishing*, Paris. 2016.

[2] N. Townsend, L. Wilson, P. Bhatnagar, K. Wickramasinghe, M. Rayner, M. Nichols. "Cardiovascular disease in Europe: epidemiological update," *Eur Heart J*2016; 37 (42): 3232-3245. 2016.

[3] T. J. Gundert, A. L. Marsden, W. Yang, D. S. Marks, J. F. LaDisa Jr, "Identification of Hemodynamically Optimal Coronary Stent Designs Based on Vessel Caliber," IEEE Transactions on Biomedical Engineering. vol: 59, Issue: 7, pp: 1992–2002. July 2012.

[4] E. Y. Chow, A. L. Chlebowski, S. Chakraborty, W. J. Chappell, P. Irazoqui, "Fully Wireless Implantable Cardiovascular Pressure Monitor Integrated with a Medical Stent," IEEE Transactions on Biomedical Engineering. vol: 57, n. 6, pp: 1487–1496. Feb: 2010.

[5] G. W. Stone *et al.*, "Comparison of a polymer-based Paclitaxerl-Eluting Stent with a Bare Metal Stent in patients with complex Coronary Artery Disease," *J. Amer. Medical Assoc.*, vol. 294, n. 10, pp. 1215-1223, 2005.

[6] S-J. Park *et al.*, "In-stent neoatherosclerosis – a final common pathway of late stent failure," *J. Amer. College Cardiology*, vol. 59, n. 23, pp. 2052-2057, 2012.

[7] J.A. Miguel, D. Rivas, Y. Lechuga, M.A. Allende, M. Martinez, "A novel computer-assisted design tool for implantable MEMS pressure sensors," Microprocessors and Microsystems, vol 46(A), pp:75-83. 2016.

[8] D. Rivas-Marchena *et al.*, "Energy-efficient implantable transmitter for restenosis monitoring with intelligent-stents," in *37th Int. Conf. IEEE Eng. Medicine Biology Soc. (EMBS)*, Milan, pp. 3323-3326. 2015.

[9] D. Rivas-Marchena, "Caracterización de bioimpedancia para la calibración de sensores de presión capacitivos MEMS en aplicaciones cardiovasculares," M.S. thesis, University of Seville, Spain, 2016.

[10] T. Süselbeck *et al.*, "In vivo intravascular electric impedance spectroscopy using a new catheter with integrated microelectrodes," *Basic Research Cardiology*, vol. 100, n. 1, pp. 28-34, 2005.

[11] F. Yang and R. Patterson, "A novel impedance-based tomography approach for stenotic plaque detection – a simulation study," *Int. J. Cardiology*, vol. 144, n. 2, pp. 279-283, 2010.

[12] N. L. Opie *et al.*, "Chronic impedance spectroscopy of an endovascular stent-electrode array," *J. Neural Eng.*, vol. 13, n. 4, 2016.

[13] L. Shedden *et al.*, "Towards a self-reporting coronary artery stent – measuring neointimal growth associated with in-stent restenosis using electrical impedance techniques," *Biosensors Bioelectron.*, vol. 26, n. 2, pp. 661-666, 2010.

[14] G. Huertas *et al.,* "The bio-oscillator: a circuit for cell-culture assays," *IEEE Trans Circuits Syst II*, vol. 62, n. 2, pp. 164–168, 2015.

[15] H. P. Schwan and C. D. Ferris, "Four-electrode null techniques for impedance measurement with high resolution," *Review of Scientific Instruments*, vol. 39, n. 4, pp. 481-485, 1968.

[16] S. Grimnes and Ø. G. Martinsen, *Bioimpedance and Bioelectricity Basics*, 3rd Ed.: Elsevier, 2014.

[17] D. A. Sverjensky, "Interpretation and prediction of triple-layer model capacitances and the structure of the oxide-electrolyte-water interface," *Geochimica et Cosmochimica Acta*, vol. 65, n. 21, pp. 3643-3655, 2001.

[18] G. Ghione and M. Goano, "Revisiting the partial-capacitance approach to the analysis of coplanar transmission lines on multilayered substrates," *IEEE Trans. Microw. Theory Tech.*, vol 51, n 9, pp. 2007-2014, 2003.

[19] R. Igreja and C. J. Dias, "Extension to the analytical model of the interdigital electrodes capacitance for a multi-layered structure," *Sensors Actuators A: Physical*, vol. 172, n. 2, pp. 392-399, 2011.

[20] S. O. P. Blume *et al.*, "Modelling the capacitance of multi-layer conductor-facing interdigitated electrode structures," *Sensors And Actuators B: Chemical*, vol. 213, pp. 423-433, 2015.

[21] C. Gabriel and S. Gabriel. (1996, Jun.) *Compilation of the dielectric properties of body tissues at RF and microwave frequencies*. [Online]. Available: http://niremf.ifac.cnr.it/docs/DIELECTRIC/Report.html

[22] A. Olmo and A. Yúfera, "Computer simulation of microelectrode based bio-impedance measurements with Comsol," in *Biodevices 2010*. pp: 178-182. 2010.